Available at: http://www.ictp.it/~pub_off IC/2005/118

United Nations Educational Scientific and Cultural Organization
and
International Atomic Energy Agency
THE ABDUS SALAM INTERNATIONAL CENTRE FOR THEORETICAL PHYSICS

INTERACTIONS OF TWO CO-PROPAGATING LASER BEAMS IN UNDERDENSE PLASMAS USING A GENERALIZED PEACEMAN-RACHFORD ADI FORM

A.I. Mahdy
Plasma and Nuclear Fusion Department, Nuclear Research Centre, Atomic Energy Authority, 13759 Cairo, Egypt
and
The Abdus Salam International Centre for Theoretical Physics, Trieste, Italy.

Abstract

A generalized Peaceman-Rachford (P-R) ADI form based on the regularized finite difference scheme is employed in order to study the interactions of two co-propagating laser beams in underdense plasmas. A numerical algorithm using the P-R ADI form is constructed for solution of coupled 2D time-dependent non-linear Shrödinger equations for quasineutral plasmas in paraxial approximation.

The ability of the form to solve the equations is discussed, and its performance in simulating phenomena associated with the interactions in the presence of pondermotive nonlinearity and relativistic nonlinearity is examined.

It is shown that the generalized P-R ADI form can accurately solve the coupled NLS equations. With simulation results, the form is shown to be suitable to simulate the interactions of two co-propagating laser beams with underdense plasma, and it can successively simulate the associated phenomena at varying conditions.

MIRAMARE – TRIESTE
December 2005

1 Introduction

The Ultra-Short Laser Plasma Interactions is a crucial and a rapidly growing field of research in plasmas physics[1]. Many research topics, such as Laser-Based Accelerator[2], High-order Harmonic Generation[3], X-ray lasers[4], and Inertial Confinement Laser Fusion (ICF)[5] are explored due to the interactions. As a result of intensive investigations carried out in the mentioned topics, new physical phenomena with wide applications in industry[6] and medicine[7] are presented, and more are expected to be explored by developing of the laser parameters, i.e., laser intensities, pulse length and reputation rate.

As a result of Chipred Pulse Amplification (CPA) technology[8], number of laser systems with muliterra watt power, more than $10^{21} W/cm^2$ intensities and subpicosecond duration rate are now available. Such developed lasers can propagate longer than the diffraction length Z_R, with little attenuation or significant energy losses. It can also deliver laser energy P more than the critical power P_{cr} required for the relativistic self-focusing, i.e., $P \gg P_{cr} = 17(\omega_0/\omega_{pe})^2$, where ω_0 is the laser frequency and ω_{pe} is the plasma frequency. In addition, such lasers have strength field exceeding 10^{11} V/m, which is the value required to oscillate the electrons at relativistic velocity.

In such new laser configuration more physics relevant to the nonlinear interactions are discovered and new research topics such as Fast Ignition Concept [9] and Pair Production[10] are opened.

One of the research topic that has received growing interest as a direct result for laser developing is the propagation of multi laser beams in plasmas[11, 12]. In the topic, two/more co-propagating/counter-propagating laser beams nonlinearly interact with underdense plasmas to produce much of complex phenomena. Our main research is devoted to study the nonlinear interactions of two co-propagating laser beams with underdense plasmas.

The topic is of a crucial interest in ICF Physics[13], where the energy transfer between the co-propagating beams via Stimulated Brillouin Scattering is a very important topic to be studied, also in Optical Spatial Solitons[14], in which the interaction between the two beams solitons is considered to be the most fascinating feature of all solitons phenomena.

In order to study nonlinear interactions of two co-propagating laser beams with underdense plasmas, an envelope equation describing the propagation of each beam is required. Number of envelope equations describing the complex propagation of the laser beams in plasmas are derived[15, 16], but in our study, an envelope equation in two dimensional co-ordinates with slowly varying approximation and including the nonlinear effects should be considered. So, a 2D time-dependent nonlinear Shrödinger equation (NLSE) derived in paraxial approximation with the pondermotive and the relativistic nonlinearity is used.

The analytical solution of the envelope equation (NLSE) is not sufficient to describe the evolution of the physical processes, so the numerical simulation is very demanding for a detailed

analysis for the propagation. Number of numerical algorithms were employed to solve the NLSE, beginning with the implicit difference scheme[17, 18], a conservative spectral method for 2D nonlinear wave type [19], Hopscotch method[20] and a new six point scheme[21] for coupled NLSE. But, the Alternating-Direction Implicit(ADI)[22] was shown to be accurate and stable to solve the NLSE and simulate the propagation in comoving frame and paraxial approximation[23], particularly, the Peaceman-Rachford ADI scheme, which showed to be suitable to solve the NLSE in solitons solution[24].

In the present research, the nonlinear interactions of two co-propagating laser beams with underdense plasmas using a generalized Peaceman-Rachford ADI form based on the regularized finite different scheme is studied. The article is organized as follows: In section 2, basic equations; coupled envelope equations and the main physical assumptions and considerations are described. In section 3, the model and numerical algorithm constructed in order to solve the equations are explained, in addition the validity and the accuracy of the form to simulate associated phenomena is discussed. Finally, in section 4, simulation results, i.e., time-evolution for the absolute amplitude and snapshots for the propagation trajectory of the interacting beams at different intensities and separation distances between the initial beam centroids are presented.

2 Basics Equations

To study the nonlinear interactions of two co-propagating laser beams with underdense plasmas, some circumstances have to be considered: the two interacting beams can merge into a single beam, split into three or more beams or remain trapped in the density channel. This can be accurately described using the following coupled envelope equations[25]:

$$2i\frac{\partial a_1}{\partial \tau} + \nabla_\perp^2 a_1 + (1 - n/\gamma)a_1 = 0 \tag{1}$$

$$2i\frac{\partial a_2}{\partial \tau} + \nabla_\perp^2 a_2 + (1 - n/\gamma)a_2 = 0 \tag{2}$$

Each equation is a 2D time-dependent nonlinear Shrödinger-type equation (NLSE). τ is the time normalized by $\omega_{pe}t/\omega_0$, a_1 and a_2 are slowly varying vector potentials, and both are normalized by mc^2/e. $\nabla_\perp^2 \longrightarrow \nabla_{yy}^2 + \nabla_{zz}^2$, y, z are the transverse co-ordinates and x is the propagation direction and all are normalized by c/ω_{pe}. n is the electron density normalized by unperturbed density, which is time varying and γ is the relativistic factor.

Both equations are derived for slowly varying envelope, i.e., $|\partial a/\partial t| \ll |\omega_0 a|$ and in paraxial approximation, i.e., $\partial/\partial x = 0$, and the following co-ordinate transformation is applied

$$(\tau, x, y, z) \rightarrow (\tau, \eta, y, z)$$

where,

$$\eta = x - (\frac{k_0 c}{\omega_{pe}})\tau$$

With the previous transformation, each equation becomes describing the propagation in co-moving frame η, where k_0 is laser wave number.

In our physical considerations, the study is carrying out for tenuous plasma, i.e., plasma far from critical density n_c, with $n/n_c \ll 0.01$, and in the equations, the nonlinear effects of the relativistic nonlinearity and the density modification by the transverse pondermotive nonlinearity are included. Certain kinetic effects such as electron acceleration, attraction of electron filamentation and corresponding qusistatic magnetic field have been neglected.

3 The Algorithm

In a previous study performed to solve a 2D heat equation[27], the author showed that the Peaceman-Rachford ADI (P-R ADI) scheme has a disadvantage to solve the equation at large heat coefficient values, and the scheme is not suitable to simulate phenomena occurred at this condition. In order to overcome the disadvantage, the author introduced a generalized P-R ADI form based on the regularized finite difference scheme, he proofed that with certain values for a control parameter, the form can successively simulate the phenomena, regardless of the heat coefficient values.

In this section, the P-R ADI scheme will be applied to solve the coupled envelope equations. The stability of the scheme and its ability to solve the equations and simulate the associated phenomena will be examined. Following that, the generalized P-R ADI form will be employed, the ability of the form to simulate the problem at varying conditions will be shown, in addition, the control parameter values required for an accurate solution will be evaluated.

3.1 Peaceman-Rachford ADI Scheme

In a P-R ADI scheme, each envelope equation (Eqs.(1) or (2)) is splitted up as

$$\frac{a_{I,J}^{n+1/2} - a_{I,J}^{n}}{\triangle t/2} = \frac{i}{2}\nabla_y^2 a_{I,J}^{n+1/2} + \frac{i}{2}\nabla_z^2 a_{I,J}^{n} + \frac{i}{2}N(a)a_{I,J}^{n+1/2} \tag{3}$$

$$\frac{a_{I,J}^{n+1} - a_{I,J}^{n+1/2}}{\triangle t/2} = \frac{i}{2}\nabla_y^2 a_{I,J}^{n+1/2} + \frac{i}{2}\nabla_z^2 a_{I,J}^{n+1} + \frac{i}{2}N(a)a_{I,J}^{n+1} \tag{4}$$

where $N(a) = (1 - n/\gamma)$, $\triangle t$ is the time step,

$$\nabla_y^2 a_{I,J} = \frac{a_{I-1,J} - 2a_{I,J} + a_{I+1,J}}{h^2} = \frac{1}{h^2}\delta_y^2$$

and

$$\nabla_z^2 a_{I,J} = \frac{a_{I,J-1} - 2a_{I,J} + a_{I,J+1}}{h^2} = \frac{1}{h^2}\delta_z^2$$

where h is the grid size, $\delta_y^2 = a(I-1,J) - 2a(I,J) + a(I+1,J)$ and $\delta_z^2 = a(I,J-1) - 2a(I,J) + a(I,J+1)$.

Let $r = (i\triangle t/4h^2)$, then Eqs.(3) and (4) will be

$$(1 - r\delta_y^2 - h^2 rN(a))a_{I,J}^{n+1/2} = (1 + r\delta_z^2)a_{I,J}^n \tag{5}$$

$$(1 - r\delta_z^2 - h^2 rN(a))a_{I,J}^{n+1} = (1 + r\delta_y^2)a_{I,J}^{n+1/2} \tag{6}$$

Eliminating $a_{I,J}^{n+1/2}$ from Eqs.(5) and (6) gives

$$(1 - r\delta_y^2 - h^2 rN(a))(1 - r\delta_z^2 - h^2 rN(a))a_{I,J}^{n+1} = (1 + r\delta_y^2)(1 + r\delta_z^2)a_{I,J}^n \tag{7}$$

To examine the stability of the P-R ADI scheme and its ability to solve the equation, let's substitute $a_{I,J}$ in Eq.(7) with the following form

$$a = a(I, J)e^{i(I+J)h\pi} = a(I, J)e^{i(\sigma_1+\sigma_2)h}$$

where $\sigma_1 = I\pi, \sigma_2 = J\pi$ and $I, J = (-N, -N + 1, ... - 3, -2, -1, , 0, 1, 2, 3, ...N - 1, N)$, then, the amplification factor for Eq.(7) will be equal to

$$G = \frac{(1 - 4r\sin^2(\frac{\sigma_1 h}{2}))(1 - 4r\sin^2(\frac{\sigma_2 h}{2}))}{(1 + 4r\sin^2(\frac{\sigma_1 h}{2}) - h^2 rN(a))(1 + 4r\sin^2(\frac{\sigma_2 h}{2}) - h^2 rN(a))} \tag{8}$$

As shown in Eq.(8), the amplification factor directly depends on σ_1, σ_2, r and $N(a)$, i.e., $I, J, \triangle t$, h and $N(a)$ values.

$N(a)$ depends on electron density n, which is time-varying and given by

$$n = \text{MAX}(0, 1 + (\nabla_y^2 + \nabla_z^2)\gamma)$$

and the relativistic factor γ, it is time-varying and defined as

$$\gamma = \sqrt{1 + |a_1|^2 + |a_2|^2}$$

From the previous definitions for n and γ, it is clear that $N(a)$ is time-varying, but in the case of n; which is addressing the pondermotice expulsion of the electron density from the high-intensity region, becomes equal to γ; which represents the electron mass correction due to the relativistic effect, then $N(a) = 0$, and in this case, the amplification factor will be modified to be

$$G = \frac{(1 - 4r\sin^2(\frac{\sigma_1 h}{2}))(1 - 4r\sin^2(\frac{\sigma_2 h}{2}))}{(1 + 4r\sin^2(\frac{\sigma_1 h}{2}))(1 + 4r\sin^2(\frac{\sigma_2 h}{2}))} \tag{9}$$

In Eq.(9), for any $r > 0$, the amplification factor $|G| < 0$. In such condition, the P-R ADI scheme will be unconditionally stable, i.e., a stable solution for the envelope equation can be achieved, consequently, an accurate simulation for the problem can be performed.

But in case of large r; depending on the simulation parameters, and at large I ans J, as an example $I = Imax = N - 1$ or $-N + 1$ and $J = Jmax = N - 1$ or $-N + 1$, the amplification factor will be

$$|G(r, Imax, Jmax)| \approx \left| \frac{(r \sin^2 \frac{Imax\,\pi h}{2})(r \sin^2 \frac{Jmax\,\pi h}{2})}{(r \sin^2 \frac{Imax\,\pi h}{2})(r \sin^2 \frac{Jmax\,\pi h}{2})} \right| \approx 1 \tag{10}$$

The result obtained in Eq.(10) shows that the scheme solution slowly converges towards the exact solution, which means, physical processes which occurred at this condition can not be accurately simulated.

This is considered as a disadvantage for the P-R ADI scheme for the case of $N(a) = 0$, and at large r, I and J, and in order to overcome this disadvantage, another form, in particular the generalized P-R ADI form is recommended to be applied.

3.2 Generalized Peaceman-Rachford ADI Form

In the generalized P-R ADI form based on the regularized finite difference scheme, each envelope equation is splitted up as

$$(1 - \frac{\epsilon i \triangle t \delta_y^2}{4h^2})(\frac{a_{I,J}^{n+1/2} - a_{I,J}^{n}}{\triangle t/2}) = \frac{i}{2h^2}\delta_y^2 a_{I,J}^{n+1/2} + \frac{i}{2h^2}\delta_z^2 a_{I,J}^{n} + \frac{i}{2}N(a)a_{I,J}^{n+1/2} \tag{11}$$

$$(1 - \frac{\epsilon i \triangle t \delta_z^2}{4h^2})(\frac{a_{I,J}^{n+1} - a_{I,J}^{n+1/2}}{\triangle t/2}) = \frac{i}{2h^2}\delta_y^2 a_{I,J}^{n+1/2} + \frac{i}{2h^2}\delta_z^2 a_{I,J}^{n+1} + \frac{i}{2}N(a)a_{I,J}^{n+1} \tag{12}$$

ϵ is small and positive parameter; control parameter, when $\epsilon = 0$ the generalized form will be in the P-R ADI scheme.

Let $r = (i\triangle t/4h^2)$, then Eqs.(11) and (12) are re-written as

$$(1 - \epsilon r\delta_y^2 - r\delta_y^2 - h^2 rN(a))a_{I,J}^{n+1/2} = (1 - \epsilon r\delta_y^2 + r\delta_z^2)a_{I,J}^{n} \tag{13}$$

$$(1 - \epsilon r\delta_z^2 - r\delta_z^2 - h^2 rN(a))a_{I,J}^{n+1} = (1 - \epsilon r\delta_z^2 + r\delta_y^2)a_{I,J}^{n+1/2} \tag{14}$$

Eliminating $a_{I,J}^{n+1/2}$ from Eqs.(13) and (14) gives

$$(1-\epsilon r\delta_y^2-r\delta_y^2-h^2 rN(a))(1-\epsilon r\delta_z^2-r\delta_z^2-h^2 rN(a))a_{I,J}^{n+1} = (1-\epsilon r\delta_y^2+r\delta_z^2)(1-\epsilon r\delta_z^2+r\delta_y^2)a_{I,J}^{n} \tag{15}$$

Substituting $a_{I,J}$ in the previous equation with $a_{I,J} = a(I,J)e^{i(\sigma_1+\sigma_2)h}$, the amplification factor becomes

$$G = \frac{(1+4\epsilon r\sin^2(\frac{\sigma_1 h}{2}) - 4r\sin^2(\frac{\sigma_2 h}{2}))(1+4\epsilon r\sin^2(\frac{\sigma_2 h}{2}) - 4r\sin^2(\frac{\sigma_1 h}{2}))}{(1+4\epsilon r\sin^2(\frac{\sigma_1 h}{2}) + 4r\sin^2(\frac{\sigma_1 h}{2}) - h^2\epsilon r N(a))(1+4r\epsilon\sin^2(\frac{\sigma_2 h}{2}) + 4r\sin^2(\frac{\sigma_2 h}{2}) - h^2 r N(a))} \tag{16}$$

The previous relation shows that the amplification factor depends on $I, J, \triangle t, h$, $N(a)$ in addition to a new parameter; the control parameter ϵ.

In the case of $N(a) = 0$, the amplification factor is modified to

$$G = \frac{(1+4\epsilon r\sin^2(\frac{\sigma_1 h}{2}) - 4r\sin^2(\frac{\sigma_2 h}{2}))(1+4\epsilon r\sin^2(\frac{\sigma_2 h}{2}) - 4r\sin^2(\frac{\sigma_1 h}{2}))}{(1+4\epsilon r\sin^2(\frac{\sigma_1 h}{2}) + 4r\sin^2(\frac{\sigma_2 h}{2}))(1+4r\epsilon\sin^2(\frac{\sigma_2 h}{2}) + 4r\sin^2(\frac{\sigma_1 h}{2}))} \tag{17}$$

It is clear in Eq.(17), the control parameter has a major impact in controlling the amplification factor value, so by a suitable selection for its values, a fast converging towards the exact solution can be achieved.

In order to determine the suitable control parameter for a stable and accurate simulations, let's put $\alpha = 4r = i\triangle t/h^2$, $\beta_1 = \sin^2(\frac{\sigma_1 h}{2})$ and $\beta_2 = \sin^2(\frac{\sigma_2 h}{2})$ in Eq.(17), then the amplification factor will be in the form

$$|G| = \left|\frac{(1-\alpha(\beta_2 - \epsilon\beta_1)}{(1+\alpha\beta_1(1+\epsilon))}\frac{(1-\alpha(\beta_1 - \epsilon\beta_2)}{(1+\alpha\beta_2(1+\epsilon))}\right| \tag{18}$$

Let's select ϵ to be

$$\epsilon = \min\{\beta_1/\beta_2, \beta_2/\beta_1\} \tag{19}$$

With the above selection, $(\beta_1 - \epsilon\beta_2) > 0$ and $(\beta_2 - \epsilon\beta_1) > 0$, and the amplification factor will be

$$|G| = \left|\frac{(1-\alpha(\beta_2 - \epsilon\beta_1))}{(1+\alpha\beta_1(1+\epsilon))}\frac{(1-\alpha(\beta_1 - \epsilon\beta_2))}{(1+\alpha\beta_1(1+\epsilon))}\right| < 1 \tag{20}$$

As shown in Eq.(20), the form is unconditionally stable, but for large α, the amplification factor is given by

$$|G| = \left|\frac{(\beta_1 - \epsilon\beta_2)}{\beta_1(1+\epsilon)}\frac{(\beta_2 - \epsilon\beta_1)}{\beta_2(1+\epsilon)}\right| < 1 \tag{21}$$

It is clearly noted in Eq.(21) that the amplification factor is un-effected by changing the α value, in addition, at varying iterations, including the large cases (large β_1 and β_2 in this case), the amplification factor is always < 1, as ϵ satisfies Eq.(19).

The above calculations and results show that depending on the control parameter value, the P-R ADI form overcomes the disadvantage of the P-R ADI scheme and it can solve the equation

and simulate the associated phenomena accurately.

As shown in Eq.(19), in order to evaluate the suitable control parameter value, it is required to calculate the ratio between β_1 and β_2, in particular at large I and J, where the form is recommended to be applied.

At large I and J or at $Imax$ and $Jmax$, this ratio has the following values:

Case 1: $I = Imax, J = \pm 1, \pm 2, \pm 3, ..., ..., ..., ...Jmax,$

$$\frac{\beta_1}{\beta_2} = \frac{\sin^2(\frac{Imax\,\pi h}{2})}{\sin^2(\frac{J\pi h}{2})} \approx O(h^2), \qquad \frac{\beta_2}{\beta_1} = \frac{\sin^2(\frac{J\pi h}{2})}{\sin^2(\frac{Imax\,\pi h}{2})} \approx O(1/h^2)$$

Case 2: $I = Imax, J = Jmax,$

$$\frac{\beta_1}{\beta_2} = \frac{\sin^2(\frac{Imax\,\pi h}{2})}{\sin^2(\frac{Jmax\,\pi h}{2})} \approxeq 1, \qquad \frac{\beta_2}{\beta_1} = \frac{\sin^2(\frac{Jmax\,\pi h}{2})}{\sin^2(\frac{Imax\,\pi h}{2})} \approxeq 1$$

Case 3: $I = \pm 1, \pm 2, \pm 3, ..., .., ...Imax, J = Jmax,$

$$\frac{\beta_1}{\beta_2} = \frac{\sin^2(\frac{I\pi h}{2})}{\sin^2(\frac{Jmax\,\pi h}{2})} \approx O(1/h^2), \qquad \frac{\beta_2}{\beta_1} = \frac{\sin^2(\frac{Jmax\,\pi h}{2})}{\sin^2(\frac{I\pi h}{2})} \approx O(h^2)$$

It is clear from the results obtained above that β_1 and β_2 ratio is in order of three possible values, which are $O(h^2), 1, O(1/h^2)$, so the suitable control parameter for an accurate simulation be given by

$$\epsilon = \min\{h^2, 1, 1/h^2\}.$$

4 Simulations Results

In our simulations, the two co-propagating laser beams are selected to have the same frequency and the polarization direction, and their initial transverse beam profiles are chosen to be Gaussian, which are govern by by following equations:

$$\begin{aligned} a_1 &= a_{01} e^{([-(y_1 - y_{01})^2 + z_1^2]/2\rho_{01})} \\ a_2 &= a_{02} e^{([-(y_2 - y_{02})^2 + z_2^2]/2\rho_{02})} \end{aligned}$$

a_{01} and a_{02} are the initial complex amplitudes of the two beams, y_{01} and y_{02} are the initial beam centroids. ρ_{01} and ρ_{02} are parameters related to the normalized threshold power for the relativistic self-focusing, their values must fulfill the relativistic self-focusing condition, i.e.,

$a_{01}^2\rho_{01}^2 \geq 16$ and $a_{02}^2\rho_{02}^2 \geq 16$, so they are given an equal and fixed value during the simulations, which is $\rho_{01} = \rho_{02}$=8.

Figure 1 shows time-evolution for the absolute amplitudes $\Sigma = \sqrt{|a_1^2| + |a_2^2|}$, for two interacting beams at $a_{01} = a_{02} = 0.4, y_{01} = 10$ and $y_{02} = -10$, as shown at $\tau = 0$.

At $\tau = 55$, two individually self-focused beams are observed, each is self-focused at high intensity around its initial centroid.

The self-focusing is a basic phenomena in the nonlinear laser propagation in plasmas, which is obtained due to two effects, namely, the pondermotive and relativistic self-focusing effect.

In the pondermotive effect, a pondermotive force is formed due to nonlinear coupling between spatially varying light beam and plasmas, the resulted force expels the electrons along the transverse direction and reduces the electrons density. In the relativistic effect, the ultra high power laser accelerates the electrons to the relativistic speed and increases their masses by the relativistic factor. Both effects reduce the plasma frequency and produce a large refractive index, as a result, the wave front of the beam rapidly converge causing the self-focusing.

At $\tau = 90$, the individual self-focusing behavior is continuing, but for focused beams with growing intensity.

At $\tau = 115$, the two beams merge into a highly focused single beam. The merging process is a result for the nonlinear mutual interactions between the co-propagating beams. The processes is obtained when the mutual attraction force between the co-propagating beams is stronger than the mutual repulsive force. The merged beam keeps its feature as a single high intense beam without changing, as shown at $\tau = 200$ and $\tau = 250$.

Figure 2 shows time-evolution for the absolute amplitudes Σ, of two beams at $a_{01} = a_{02} = 0.6, y_{01} = 10$, and $y_{02} = -10$, as shown at $\tau = 0$.

At $\tau = 30$, two individually self-focused beams are observed, each beam is self-focused around its initial centroid.

It may be noted that, at $\tau = 30$ the interacting beams are self-focused earlier comparing with the case in figure 1. The reason for the earlier self-focusing is attributed to the difference between the applied complex amplitudes in both cases. Here a higher amplitude is applied, and a higher amplitude leads to stronger evacuation for the electrons by the pondermotive force and increasing to the electron masses due to the relativistic effect. As a result, fast converging for the beam wave front is performed, consequently, quick self-focusing is obtained.

At $\tau = 75$, in addition to the two individually highly intense self-focused beams, a third beam with lower intensity located between the two main beams is observed. The formation of the third beam is a direct impact for a nonlinear mutual interactions between the co-propagating beams, and the continuity of this beam depends on the balance between the mutual attractive and repulsive forces between the main beams. In case of a stronger attractive force than repulsive

one, the formed beam can sustain and grow, but in case of a stronger repulsive force than attractive one, the formed beam can be channeled by the main beams and disappear.

At $\tau = 135$, the channeling of the third beam by the main beams is observed, which indicates that the repulsive force is stronger than the attractive force in this stage.

At $\tau = 180$, the main beams remain individually self-focusing, but each is self-focused far from its initial centroid, in opposite directions, this indicates that the repulsive force is still stronger than the attractive one.

The growing of the repulsive force is continuing, where the two beams are propagating away from each other, and the separation distance between their centroids is increasing, as it is clearly shown at $\tau = 215$.

Figure 3 shows a snapshot of the propagation trajectory of the absolute amplitudes Σ, of two interacting beams at $a_{01} = a_{02} = 0.6, y_{01} = 10$ and $y_{02} = -10$.

At $\tau \approx 25$, the two beams start to self-focus at high intensity and small spot size, afterward, they start to attract each other and propagate in a slightly shifted trajectory.

At $\tau \approx 50$, the two beams split into three beams, a center one at low intensity and two self-focused at high intensity. The center one propagates along its main trajectory to be completely defocused at $\tau \approx 100$, while the two self-focused at constant intensity start to repel each other, where the separation distances between their centroids is gradually increasing.

The self-focused beams produce strong electron-density cavitation, which prevent the beams to merge into a single beam, so they propagate in repulsive propagation trajectory with constant intensity and spot size as shown from $\tau \approx 100$ to the final stage.

Figure 4 shows time-evolution for the absolute amplitude Σ, of two interacting beams at $a_{01} = a_{02} = 0.8, y_{01}$=10 and $y_{02} = -10$, as shown at $\tau = 0$.

At $\tau = 45$, it is shown that two individually self-focused beams, each is self-focused at high intensity around its initial centroid, in addition, a lower intensity beam in the middle of the main beams is formed.

This configuration is previously observed in figure 2, but here, the configuration is formed more quickly and at higher intensity than the previous one.

The mechanism of the formation of such configuration has been explained before, and the reason for the faster formation and the higher intensity is due to the higher amplitude applied in this case.

At $\tau = 110$, a new configuration is shown, multi-beams or multiple filaments structure for more than three beams is observed.

The Multiple filaments structure was previously observed in the nonlinear single laser beam propagation in plasmas[28]. The structure is resulted when the beam is self-focused above the critical power for collapse, and as a result, the single beam breaks up into multi narrow single

filaments. The structure depends on the initial power and intensity configuration of the single beam.

At $\tau = 155$, the multiple filaments structure is observed, but here the separation distances between the beam centroids are longer and the intensity of the middle beams is higher.

At $\tau = 205$, the multiple filaments structure is continuing, but the separation distances between their centroids are growing longer, and the middle beam is channeled by the main beams. This indicates that the mutual repulsive force is growing stronger than the mutual attractive force, and it is more dominate force at this stage as shown at $\tau = 225$.

Figure 5 shows the propagation trajectory of the absolute amplitude Σ, of two interacting beams at $a_{01} = a_{02} = 0.8, y_{01} = 12$, and $y_{02} = -12$.

It is noted in the presented snapshot that the mutual interactions between the main co-propagating beams, either the mutual attractive force in the early stage or the mutual repulsive force in the advanced stage, are relatively weak.

The reason for the weak forces is due to the increasing of the separation distance between the initial beam centroids here, and this increasing mainly reduce the effects of the mutual interactions between the beams.

It is also noted in the present snapshot, the absence of the multiple filaments structure, although it is observed in the figure, where the separation distance between the initial beam centroids is shorter.

The disappearance of the multiple filaments structure here is also attributed to increasing the separation distance between the initial beam centroids, consequently reducing the mutual interactions forces between the beams.

Figure 6 shows the propagation trajectory of the absolute amplitude Σ, of two interacting beams at $a_{01} = a_{02} = 1, y_{01} = 10$, and $y_{02} = -10$.

Number of complex processes are observed here. At $\tau \approx 20$, two beams are self-focused and attract each other, while at $\tau \approx 40$, the two beams change their propagation trajectory and start to repel each other, and at $\tau \approx 100$, they re-attract each other again.

At this stage, the unstable propagation trajectory is clearly observed, this unstable trajectory is resulted due to the hosing instability, which is caused due to the mutual attraction and density cavitation.

At $\tau \approx 120$, the two beams merge into a single beam, but before the merging processes, it is noted that the two beams are completely defocused and during the merging processes, strong radiation is emitted. Finally, a single beam at high intensity and constant spot size is formed which propagates in stable trajectory without changing or defocusing.

5 Conclusion

The generalized P-R ADI form based on the regularized finite difference scheme is shown to be efficient to simulate the interactions of two laser beams co-propagating in underdense plasmas. The governing equations; the coupled 2D time-dependent NLSE for tenuous plasma in paraxial approximation are accurately solved using the form. The form is shown to be unconditionally stable to solve the equations, and at large iterations when pondermotive expulsion term becomes closer to the relativistic factor, the form is shown to overcome the slowly converging towards the exact solution.

With time-evolution for the absolute amplitude of the two interacting beams at different laser parameters, the basic phenomena associated with the interactions, such as: beam self-focusing, mutual beam attraction, mutual beam repulsion, beams merging into a single beam, beam splitting into more than two beams are clearly observed. In the snapshots for the absolute amplitude of the propagation trajectory of the beams, strong emission of radiation during the merging, beam trapping due to electron-density cavitation, stable and unstable propagation trajectory (hosing propagation) are detected.

Acknowledgments

The author would like to thank the Abdus Salam International Centre for Theoretical Physics, Trieste, Italy, for providing the opportunity to visit the Centre and use its facilities to carry out this research.

References

[1] P. Gibbon and E. Förster, Plasma Phys. Control. Fusion 38 (1996) 769.

[2] E. Esarey, P. Sprangle, J. Krall and T. Ting, IEEE Transaction on Plasma Science 24, (1996) 252.

[3] P. Gibbon, IEEE J. Quantum Electron. 33, (1997) 1915.

[4] D.L. Mattews, et al., Phys. Rev. Lett. 54, (1985) 110.

[5] J.D. Lind, Phys. Plasmas 2, (1995) 3933.

[6] J.H. Booth, Thin Solid Films 453, (2004) 450.

[7] S.V. Bulanov, and V.S. Khoroshkov, Plasmas Phys. Rep. 28, (2002) 453.

[8] D. Strickland and G. Mourou, Opt. Commun. 56, (1985) 219.

[9] M. Tabak, J. Hammer, M.E. Glinsky, W.L. Kruer, S.C. Wilks, J.Woodworth, E.M. Campbell, M.D. Perry, and R.J. Mason, Phys. Plasmas 1, (1994) 1626.

[10] E.P. Liang, S.C. Wilks, and M. Tabak, Phys. Rev. Lett. 81, (1999) 4887.

[11] H.C. Wu, Z.M. Sheng, and J. Zhang, Phys. Rev. E. 70, (2004) 26407.

[12] Z.M. Zheng, K. Mima, J. Zhang, and J. Meyer-te-Vehn, Phys. Rev. E. 69, (2004) 16407.

[13] W.L. Kruer et al., Phys. Plasmas 3, (1996) 382.

[14] G.I.A. Stegeman, D. N. Christodoulides, and M. Segev, IEEE on Selected Topics in Qunt. Electron. 6, (2000) 1419.

[15] E. Esarey, J. Krall. and P. Sprangle, Phys. Rev. Lett. 72 (1994) 2887.

[16] R.A. Cairns, A. Reitsma, and E. Bingham, Phys. of Plasmas 11, (2004) 766.

[17] A.L.Dyshko, V.N. Lugovoi, and A.M. Prokhorov, JETP. Lett. 6, (1967) 146.

[18] J.I. Ramos, Appl. Math. and Comp. 133, (2002) 1.

[19] B.-F. Feng, T. Kawahara, and T. Mitsui, J. of Comp. Phys. 153, (1999) 467.

[20] S.C. Tsang, and K.W. Chow, Math. Comput. Simul. 66, (2004) 551.

[21] J. Sun, X. Gu, and Z. Ma, Physica D 196, (2004) 311.

[22] W.H. Press, S.A. Teukolsky, W.T. Vetterling, and B.P. Flannery, Numerical Recipes in Fortran (Cambridge University Press, New York, 1992) p. 861.

[23] X.L. Chen and R.N. Sudan Phys. Fluids B 5, (1993) 1336.

[24] T. Zhang, Q. Cao, G.W. Price, K. Djidjeli, and E.H. Twizell, Appl. Math. J. Chinese Univ. Ser. B. 14, (1999) 21.

[25] Q.-L. DONG, Z.-M. Sheng, and J. Zhang, Phys. Rev. E 66, (2002) 27402.

[26] Z.-M.Sheng, K. Nishihara, T. Honda, Y. Sentoku, and K. Mima, and S.V. Bulanov, Phys. Rev. E 64, (2001) 66409.

[27] W. Dai, J. of Sci. Comput. 12, (1997) 353.

[28] A.B. Borisov, O.B. Shiryaev, A. McPherson, K. Boyer, and C.K. Rhodes, Plasma Phys. Control. Fusion 37,(1995) 569.

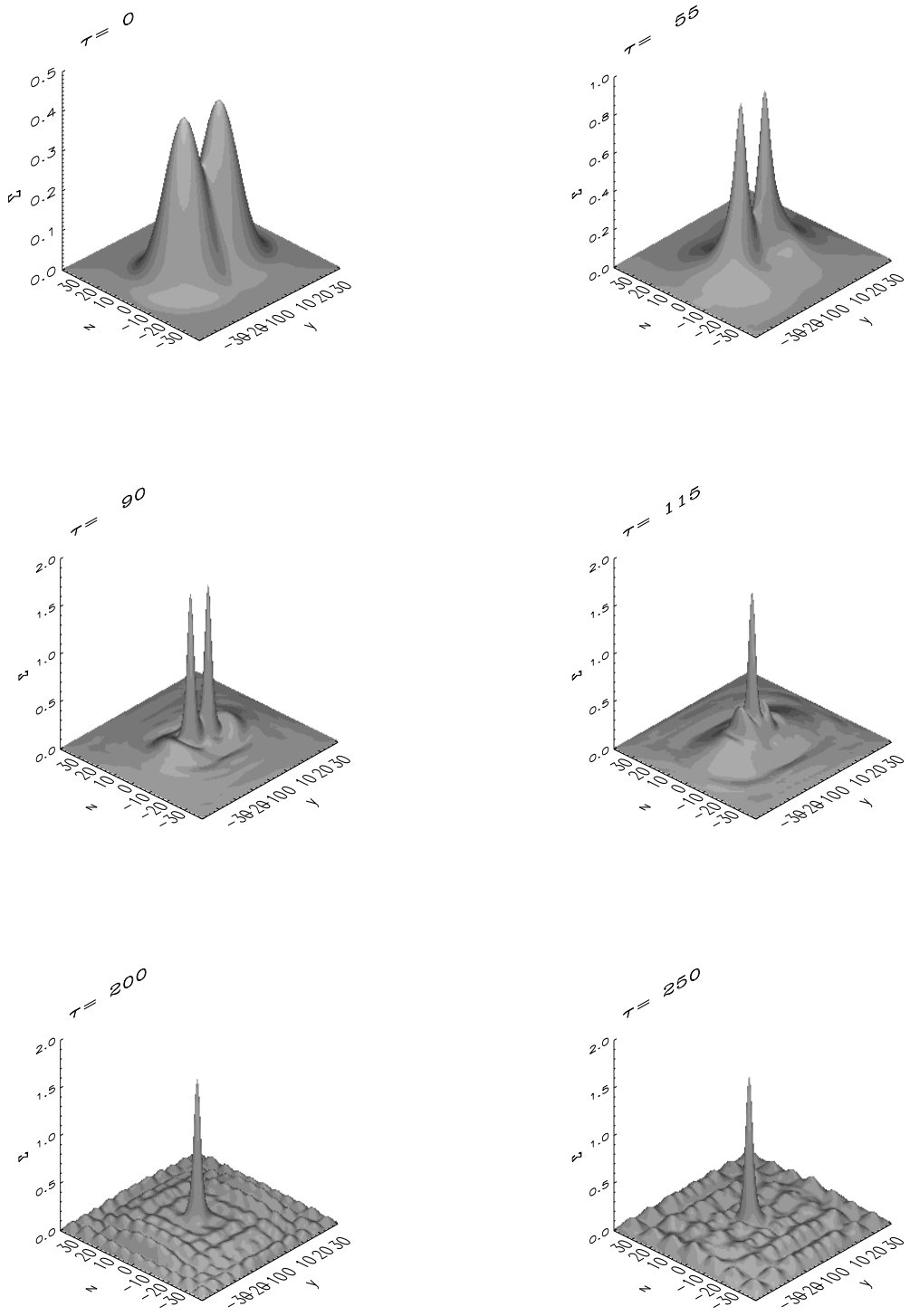

Figure 1: Time-evolution for the absolute amplitude of two co-propagating beams $(|a_1|^2 + |a_2|^2)^{1/2}$, at $a_{01} = a_{02}$=0.4, y_{01} =10, y_{02}=-10.

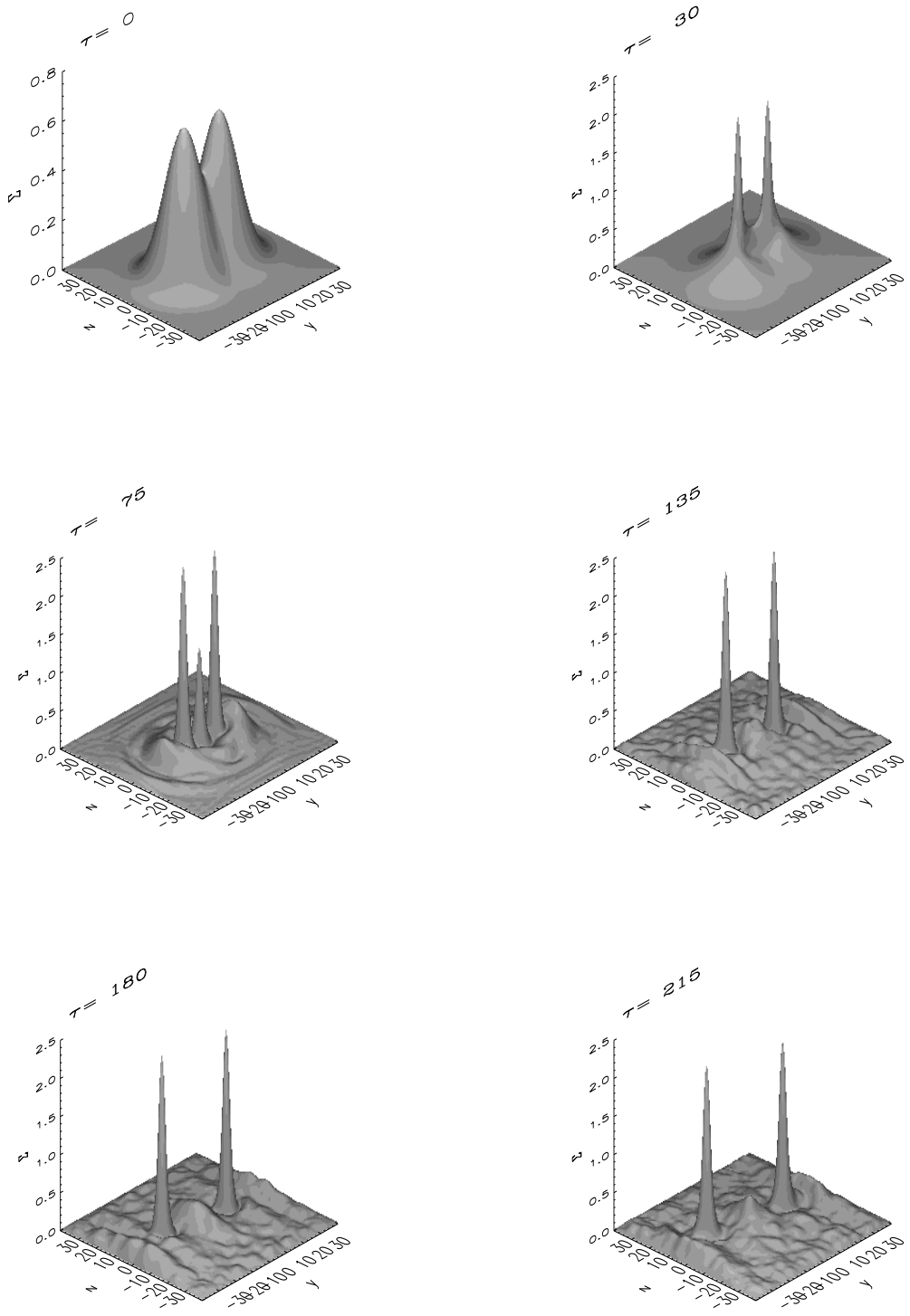

Figure 2: Time-evolution for the absolute amplitude of two co-propagating beams $(|a_1|^2 + |a_2|^2)^{1/2}$, at $a_{01} = a_{02}$=0.6, y_{01}=10, y_{02}=-10.

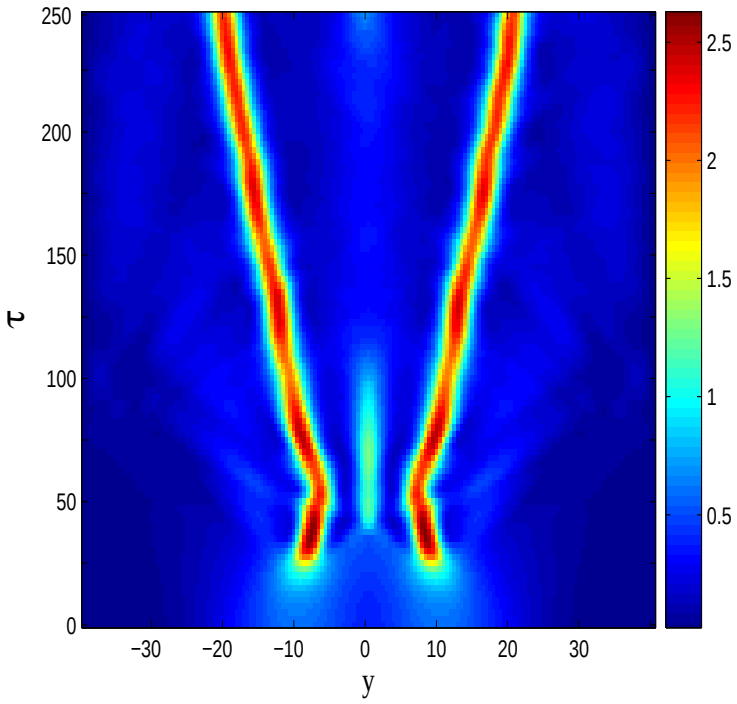

Figure 3: The propagation trajectory of the absolute amplitude of two interacting beams $(|a_1|^2 + |a_2|^2)^{1/2}$, at $a_{01} = a_{02} = 0.6, y_{01} = 10$, and $y_{02} = -10$.

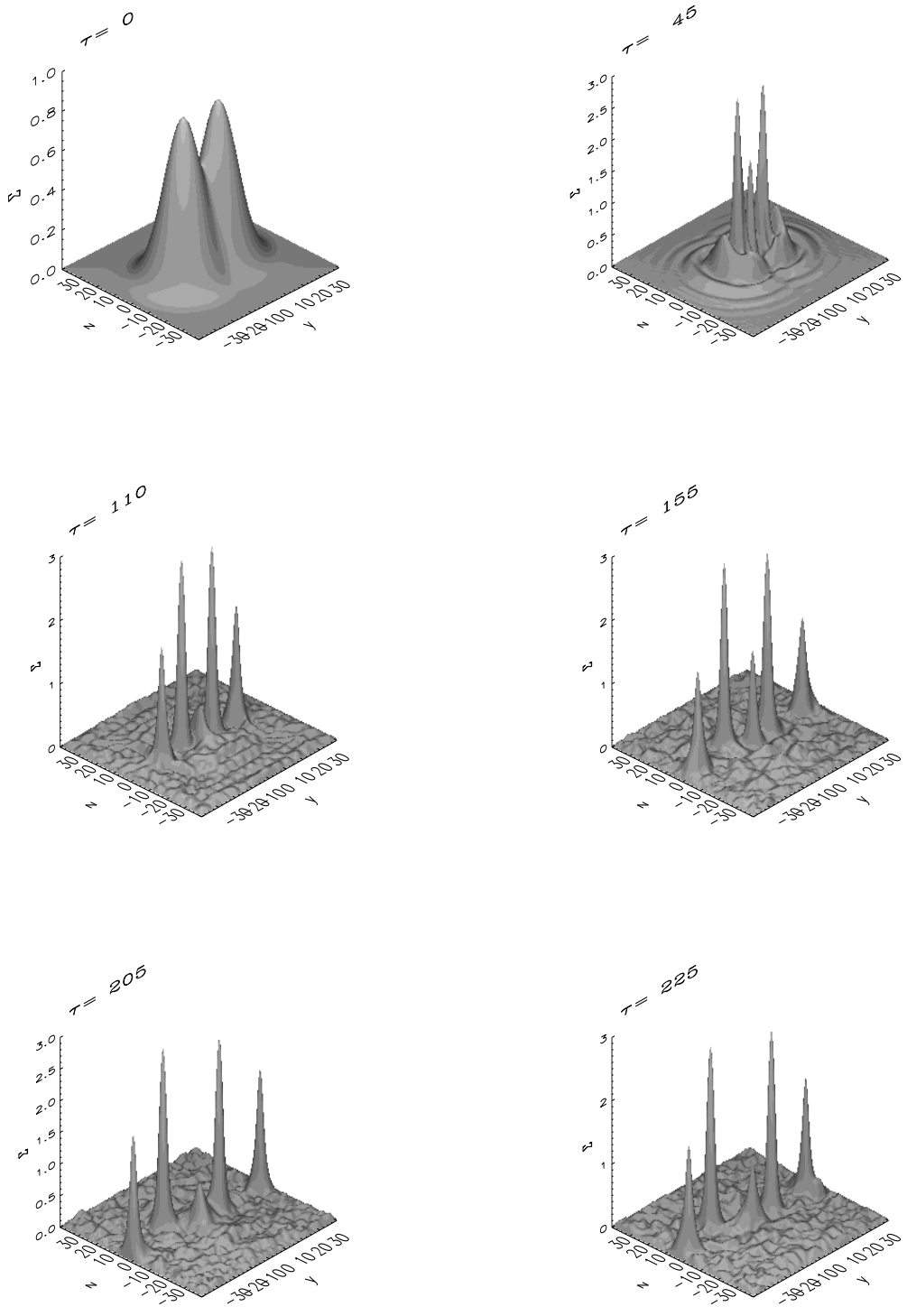

Figure 4: Time-evolution for the absolute amplitude of two co-propagating beams $(|a_1|^2 + |a_2|^2)^{1/2}$, at $a_{01} = a_{02}$=0.8, y_{01}=10, y_{02}=-10.

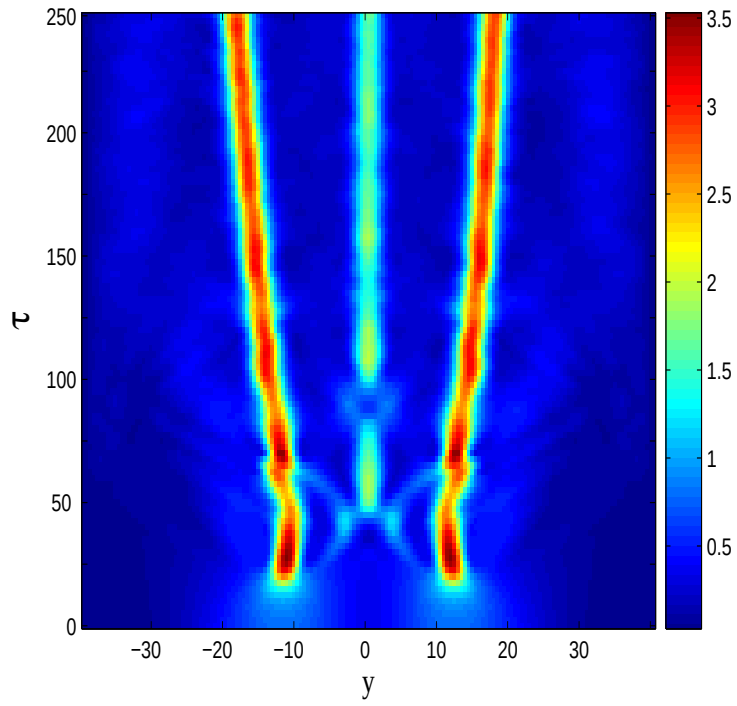

Figure 5: The propagation trajectory of the absolute amplitude of two interacting beams $(|a_1|^2 + |a_2|^2)^{1/2}$, at $a_{01} = a_{02} = 0.8, y_{01} = 12$, and $y_{02} = -12$.

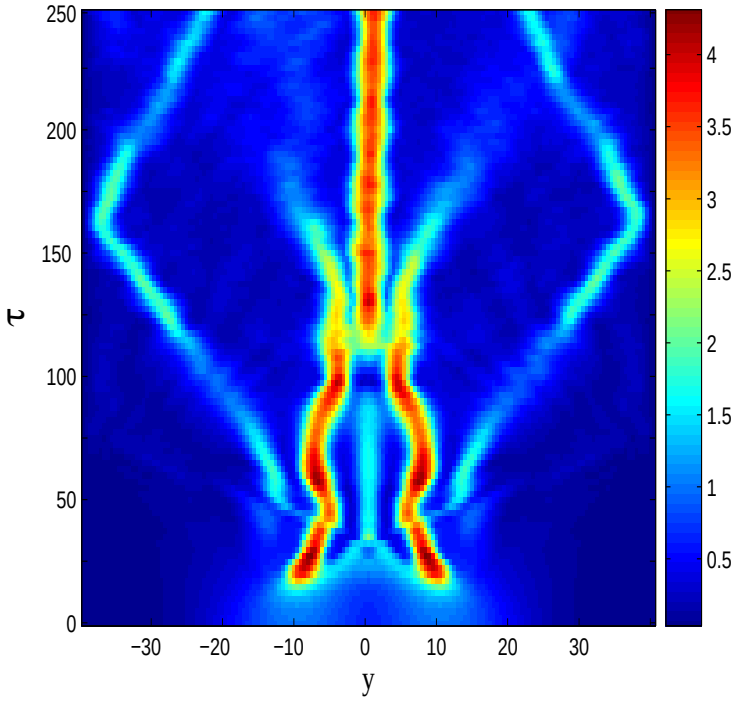

Figure 6: The propagation trajectory of the absolute amplitude of the interacting beams $(|a_1|^2 + |a_2|^2)^{1/2}$, at $a_{01} = a_{02} = 1, y_{01} = 10$, and $y_{02} = -10$.